Transition of correlated-electron emission in nonsequential double ionization of Ar atoms

Zilong Zhang,[1] **Jingtao Zhang,**[1,*] **Lihua Bai,**[2] **and Xu Wang**[3]

[1]*Department of Physics, Shanghai Normal University, Shanghai 200234, China*
[2]*Department of Physics, Shanghai University, Shanghai 200444, China*
[3]*J. R. Macdonald Laboratory, Physics Department, Kansas State University, Manhattan, Kansas 66506-2604, USA*
[*]*jtzhang@shnu.edu.cn*

Abstract: Emission of the two electrons released from nonsequential double ionization of argon atoms is anticorrelated at lower laser intensities but is correlated at higher laser intensities. Such a transition is caused by the momentum change of recollision-induced-ionization (RII) electrons. At lower laser intensities, the Coulomb repulsion between the two RII electrons dominates the motion of electrons and pushes them leaving the laser field back-to-back. At higher laser intensities, the drift momentum obtained from the laser field dominates the motion of electrons and drives them leaving the laser field side-by-side.

© 2015 Optical Society of America

References and links

1. P. B. Corkum and F. Krausz, "Attosecond science," Nat. Phys. **3**, 381 (2007).
2. S. X. Hu, "Boosting photoabsorption by attosecond control of electron correlation," Phys. Rev. Lett. **111**, 123003 (2013).
3. A. L'Huillier, L. A. Lompre, G. Mainfray, and C. Manus, "Multiply charged ions formed by multiphoton absorption processes in the continuum," Phys. Rev. Lett. **48**, 1814–1817 (1982).
4. D. N. Fittinghoff, P. R. Bolton, B. Chang, and K. C. Kulander, "Observation of nonsequential double ionization of helium with optical tunneling," Phys. Rev. Lett. **69**, 2642–2645 (1992).
5. E. Eremina, X. Liu, H. Rottke, W. Sandner, M. G. Schatzel, A. Dreischuh, G. G. Paulus, H. Walther, R. Moshammer, and J. Ullrich, "Influence of molecular structure on double ionization of N_2 and O_2 by high intensity ultrashort laser pulses," Phys. Rev. Lett. **92**, 173001 (2004).
6. S. L. Haan, L. Breen, A. Karim, and J. H. Eberly, "Recollision dynamics and time delay in strong-field double ionization," Opt. Express **15**, 767–778 (2007).
7. J. Guo, X.-S. Liu, and S.-I. Chu, "Exploration of nonsequential-double-ionization dynamics of Mg atoms in linearly and circularly polarized laser fields with different potentials," Phys. Rev. A **88**, 023405 (2013).
8. J. B. Watson, A. Sanpera, D. G. Lappas, P. L. Knight, and K. Burnett, "Nonsequential double ionization of helium," Phys. Rev. Lett. **78**, 1884–1887 (1997).
9. Th. Weber, H. Giessen, M. Weckenbrock, G. Urbasch, A. Staudte, L. Spielberger, O. Jagutzki, V. Mergel, M. Vollmer, and R. Döner, "Correlated electron emission in multiphoton double ionization," Nature (London) **405**, 658–661 (2000).
10. A. Rudenko, V. L. B. de Jesus, Th. Ergler, K. Zrost, B. Feuerstein, C. D. Schröter, R. Moshammer, and J. Ullrich, "Correlated two-electron momentum spectra for strong-field nonsequential double ionization of He at 800 nm," Phys. Rev. Lett. **99**, 263003 (2007).
11. A. Staudte, C. Ruiz, M. Schöffler, S. Schössler, D. Zeidler, Th. Weber, M. Meckel, D. M. Villeneuve, P. B. Corkum, A. Becker, and R. Dörner, "Binary and recoil collisions in strong field double ionization of helium," Phys. Rev. Lett. **99**, 263002 (2007).

12. B. Bergues, M. Kubel, N. G. Johnson, B. Fischer, N. Camus, K. J. Betsch, O. Herrwerth, A. Senftleben, A. M. Sayler, T. Rathje, T. Pfeifer, I. Ben-Itzhak, R. R. Jones, G. G. Paulus, F. Krausz, R. Moshammer, J. Ullrich, and M. F. Kling, "Attosecond tracing of correlated electron-emission in non-sequential double ionization," Nat. Commun. **3**, 813–818 (2012).

13. Y. Liu, S. Tschuch, A. Rudenko, M. Dürr, M. Siegel, U. Morgner, R. Moshammer, and J. Ullrich, "Strong-field double ionization of Ar below the recollision threshold," Phys. Rev. Lett. **101**, 053001 (2008).

14. Y. Liu, D. Ye, J. Liu, A. Rudenko, S. Tschuch, M. Durr, M. Siegel, U. Morgner, Q. Gong, R. Moshammer, and J. Ullrich, "Multiphoton double ionization of Ar and Ne close to threshold," Phys. Rev. Lett. **104**, 173002 (2010).

15. A. Emmanouilidou, "Recoil collisions as a portal to field-assisted ionization at near-uv frequencies in the strong-field double ionization of helium," Phys. Rev. A **78**, 023411 (2008).

16. D. F. Ye and J. Liu, "Strong-field double ionization at the transition to below the recollision threshold," Phys. Rev. A **81**, 043402 (2010).

17. T. Shaaran, M. T. Nygren, and C. Figueira de Morisson Faria, "Laser-induced nonsequential double ionization at and above the recollision-excitation-tunneling threshold," Phys. Rev. A **81**, 063413 (2010).

18. X. L. Hao, W. D. Li, J. Liu, and J. Chen, "Effect of the electron initial longitudinal velocity on the nonsequential double-ionization process," Phys. Rev. A **83**, 053422 (2011).

19. X. Y. Jia, X. L. Hao, D. H. Fan, W. D. Li, and J. Chen, "S-matrix and semiclassical study of electron-electron correlation in strong-field nonsequential double ionization of Ne," Phys. Rev. A **88**, 033402 (2013).

20. P. J. Ho, R. Panfili, S. L. Haan, and J. H. Eberly, "Nonsequential double ionization as a completely classical photoelectric effect," Phys. Rev. Lett. **94**, 093002 (2005).

21. B. Feuerstein, R. Moshammer, D. Fischer, A. Dorn, C. D. Schroter, J. Deipenwisch, J. R. Crespo Lopez-Urrutia, C. Hohr, P. Neumayer, J. Ullrich, H. Rottke, C. Trump, M. Wittmann, G. Korn, and W. Sandner, "Separation of recollision mechanisms in nonsequential strong field double ionization of Ar: the role of excitation tunneling," Phys. Rev. Lett. **87**, 043003 (2001).

22. W. Becker, X. Liu, P. Ho, and J. H. Eberly, "Theories of photoelectron correlation in laser-driven multiple atomic ionization," Rev. Mod. Phys. **84**, 1011–1041 (2012).

23. A. Becker and F. H. M. Faisal, "Interpretation of momentum distribution of recoil ions from laser induced non-sequential double ionization," Phys. Rev. Lett. **84**, 3546–3549 (2000).

24. R. Panfili and J. H. Eberly, "Comparing classical and quantum dynamics of strong-field double ionization," Opt. Express **8**, 431–435 (2001).

25. W. C. Liu, J. H. Eberly, S. L. Haan, and R. Grobe, "Correlation effects in two-electron model atoms in intense laser fields," Phys. Rev. Lett. **83**, 520–523 (1999).

26. J. S. Parker, B. J. S. Doherty, K. T. Taylor, K. D. Schultz, C. I. Blaga, and L. F. DiMauro, "High-energy cutoff in the spectrum of strong-field nonsequential double ionization," Phys. Rev. Lett. **96**, 133001 (2006).

27. X. Wang and J. H. Eberly, "Effects of elliptical polarization on strong-field short-pulse double ionization," Phys. Rev. Lett. **103**, 103007 (2009).

28. Y. Zhou, C. Huang, Q. Liao, and P. Lu, "Classical simulations including electron correlations for sequential double ionization," Phys. Rev. Lett. **109**, 053004 (2012).

29. S. L. Haan, Z. S. Smith, K. N. Shomsky, and P. W. Plantinga, "Anticorrelated electrons from weak recollisions in nonsequential double ionization," J. Phys. B **41**, 211002 (2008).

30. R. Panfili, S. L. Haan, and J. H. Eberly, "Slow-down collisions and nonsequential double ionization in classical simulations," Phys. Rev. Lett. **89**, 113001 (2002).

31. C. Huang, Y. Zhou, Q. Zhang, and P. Lu, "Contribution of recollision ionization to the cross-shaped structure in nonsequential double ionization," Opt. Express **21**, 11382 (2013).

32. Q. Su and J. H. Eberly, "Model atom for multiphoton physics," Phys. Rev. A **44**, 5997–6008 (1991).

33. Z. L. Zhang, L. H. Bai, and J. T. Zhang, "Double ionization of Ar below the recollision threshold intensity," Phys. Rev. A **90**, 023410 (2014).

1. Introduction

Electron correlation is the core of attoscience and molecular tomography [1], and is also important to the study of electronic motion in chemical reactions. Nonsequential double ionization (NSDI) provides a process to study and control the electron correlation [2]. During the past decades, numerous studies on NSDI have attempted to reveal electron-electron correlation in atoms and molecules [3–7]. A strong electron correlation exists in the process of NSDI [8,9]. It is generally accepted that one electron is first released by the laser field, then is driven back to its parent ion when the electric field inverses, and finally recollides with other electrons and knocks out a second electron. Electron recollision plays a key role in NSDI.

Longitudinal momentum distribution of the correlated electrons is the principal tool to reveal

electron correlation in NSDI and is frequently studied. Many characteristic features, such as the fingerlike structure [10,11] and the cross structure [12], are shown and studied. Because the motion of electrons in a laser pulse depends on the laser intensity, the longitudinal momentum distribution varies distinctively with the laser intensity. It has been shown that the longitudinal momentum distribution exhibits an anticorrelation feature at lower laser intensities [13,14], but a correlation feature when the laser intensity is higher than the recollision threshold [15]. Such a transition is attributed to the quantum tunnelling effect [16,17] or the multiple recollision during the ionization process of the second electron [18–20]. Here the anticorrelation feature denotes the two electrons emitted back-to-back so that the second and the fourth quadrants of the momentum diagram are highlighted, while the correlation feature means the side-by-side emission being dominant. Seeking for the physical origin of the transition provides a deep insight into the electron correlation in intense laser fields.

According to the time interval between recollision and double ionization, two recollision mechanisms are generally identified in NSDI [21]. In the recollision-impact-ionization (RII) mechanism, the second electron is released shortly after the recollision (generally less than $0.1T$, here T denotes the optical period). In the recollision-induced-excitation-with-subsequent ionization (RESI) mechanism, the second electron is first excited then is ionized after a time interval that can be several optical periods. Hence the electric field acting on the emitted electrons may be quite different, so are the drift momenta that the emitted electrons obtain from the laser pulse. Because the drift momentum depends on the instantaneous electric field at the time of ionization, the subsequent motion as well as the momentum distribution for the RII and the RESI electrons are notably different. Deep insights into NSDI that distinguish the RII and the RESI electrons are necessary.

Various theoretical approaches have achieved great successes in NSDI [22–24]. The numerical solution to time-dependent Schrödinger equation (TDSE) is one of them [25]. However, to solve the TDSE for two electrons numerically needs much demanding resources so that it is confined to the limited NSDI cases [26]. A classical ensemble method based on the time-dependent Newton equation (TDNE) uncovers many important features of NSDI [27–29]. Detailed dynamics can be followed by trajectory back analysis [30], which allows one to study the RII and the RESI electrons separately [31].

In this paper, we use the TDNE method to study the NSDI of Ar atoms in a linearly polarized laser pulse, and focus on the transition of the longitudinal momentum distribution from anticorrelation to correlation at different laser intensities. We choose the laser intensity ranging from 5.0×10^{13} W/cm^2 to 2.0×10^{14} W/cm^2. Trajectory back analysis is performed [30], which makes us to study the RII and the RESI electrons individually. We produce the longitudinal momentum distributions of the RII and the RESI electrons, respectively. We will show that as the laser intensity increases, the RESI electrons always exhibit an uniform distribution in four quadrants of the momentum distribution diagram, while the RII electrons change their emission priority from the anticorrelation to correlation. By following the instantaneous momentum distribution of the RII electrons, we find that the Coulomb repulsion between the two RII electrons contributes mainly to the anticorrelation feature, and that the drift momentum is responsible for the correlation feature in the longitudinal momentum distributions.

2. Simulation description

The Hamiltonian of a two-active-electron atom driven by a short laser pulse is given by (atomic units are used throughout unless otherwise stated)

$$H = H_e + (\mathbf{r}_1 + \mathbf{r}_2) \cdot \mathbf{E}(t), \tag{1}$$

where H_e is the field-free Hamiltonian of the atom [32]

$$H_e = \sum_{i=1,2} \left[\frac{\mathbf{P}_i^2}{2} - \frac{2}{\sqrt{r_i^2 + a^2}} \right] + \frac{1}{\sqrt{r_{12}^2 + b^2}}, \qquad (2)$$

in which $\mathbf{r}_i$ and $\mathbf{p}_i$ denote, respectively, the position and momentum of the ith electron; r_{12} is the distance between two electrons. We use the soft-core potential and set $a = 1.5$ and $b = 0.05$ to match the ground state energy of Ar atoms. In Eq. (1), $\mathbf{E}(t)$ is the electric field of the laser pulse, and is given by $\mathbf{E}(t) = E_0 f(t) \cos(\omega t)\hat{\mathbf{x}}$, where E_0 and ω are the laser amplitude and frequency, respectively, and $\hat{\mathbf{x}}$ is a unit vector along laser polarization. The pulse envelope function $f(t)$ is chosen as a (3+10+3)-cycle trapezoidal shape in our simulation.

The motion of two electrons is governed by the TDNE as follows

$$\frac{d\mathbf{r}_i}{dt} = \frac{\partial H}{\partial \mathbf{p}_i}, \quad \frac{d\mathbf{p}_i}{dt} = -\frac{\partial H}{\partial \mathbf{r}_i}, \qquad (3)$$

where $i = 1,2$. The above TDNE is solved by employing the standard 4-5th Runge-Kutta algorithm. The original distributions of two electrons in position and momentum space are obtained with a Gaussian random series ensuring that the total energy given by Eq. (2) is -1.595 a.u. Then these electrons move for a sufficiently long time, governed by the field-free Hamiltonian, until they keep the stable position and momentum distribution. Thus we get the initial states of the ensemble. From a given initial state, the motion of two electrons in the laser pulse is governed by Eq. (3). At the end of the laser pulse, a DI event is counted when the energies of both electrons are positive. At lower laser intensities, the sequential DI rate is negligible when compared with NSDI rate, hence we treat all DI as the NSDI events. Both the initial and final states of the NSDI electrons are recorded in order, and the trajectory back analysis [30] can be performed. According to the time interval of recollision and DI, we classify the RII and the RESI events.

3. Results and discussions

We study the NSDI for Ar atoms irradiated by the laser pulse of 795 nm wavelength. The laser intensity varies from 5.0×10^{13} W/cm^2 to 2.0×10^{14} W/cm^2. We focus on the transition of the longitudinal momentum distribution from anticorrelation to correlation at different laser intensities.

Figure 1(a) depicts the momentum distribution for the laser intensity of 7.5×10^{13} W/cm^2, in which the highlighted island-like areas appear principally in the second and the fourth quadrants. This anticorrelation feature indicates more electrons ejected back-to-back. The electrons distribute mainly along the anti-diagonal, which indicates that the values of the final momenta of the two electrons are close. The ratio of electrons in the first and the third quadrants to that in the second and the fourth quadrants is about 0.863 : 1. This phenomenon agrees well with the recent experimental observation [14]. Figure 1(b) depicts the momentum distribution for 9×10^{13} W/cm^2. From this figure we see that besides the two highlighted island-like areas, small bright areas become notable in the first and the third quadrants. This indicates that the back-to-back emission is still dominant, but the side-by-side emission becomes remarkable. In this case, the momentum distribution is still anticorrelated. The ratio of electrons in the first and the third quadrants to that in the second and the fourth quadrants increases to about 0.967 : 1. This ratio increases further with the laser intensity, and reaches 1.070 : 1 for 1.0×10^{14} W/cm^2, meaning that the side-by-side electrons overcount the back-to-back electrons. This change also appears in the longitudinal momentum distribution, as shown in Fig. 1(c), in which the fingerlike structure becomes obvious in the first and the third quadrants. This structure indicates

the correlation feature being notable. Figure 1(d) depicts the longitudinal momentum distribution for 2×10^{14} W/cm^2, which exhibits notable fingerlike structures in the first and the third quadrants. The highlighted regions in the second and the fourth quadrants shrink greatly. This indicates that the back-to-back emission fades away and the side-by-side emission becomes dominant. Most electrons distribute in the first and the third quadrants. The ratio of electrons in the first and the third quadrants to that in the second and the fourth quadrants reaches 1.202 : 1.
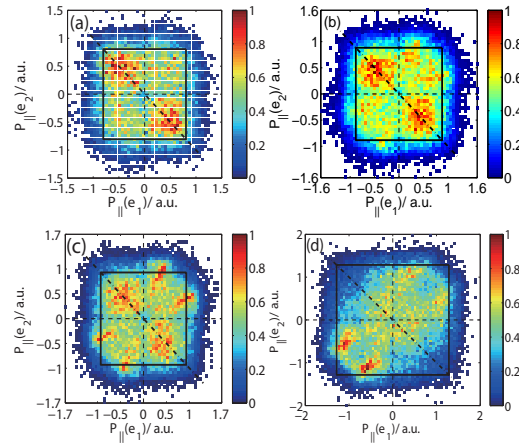

Fig. 1. Longitudinal momentum distributions of the two correlated electrons in NSDI of Ar by laser pulses of intensity (a) 0.75, (b) 0.9, (c) 1.0, and (d) 2.0×10^{14} W/cm^2, respectively. The black boxes indicate $2\sqrt{U_p}$ boundary where U_p is the ponderomotive energy. The dash-dot lines represent $y = -x$ diagonal.

It is clear that the electron emission is anticorrelated at lower laser intensities, but becomes correlated as the laser intensity increases. Such a transition is observed in [13,15] and is attributed to quantum tunnelling effect [16,17] or multiple recollision during the ionization process of the second electron [18–20]. However, recently we showed that the quantum tunnelling effect is not always important in NSDI [33]. In order to further analyze this transition, we separate the NSDI electrons into the RESI and the RII electrons, and study their momentum distributions respectively. Figs. 2(a)–2(c) depict the longitudinal momentum distributions for the RESI electrons at three laser intensities. The RESI electrons distribute uniformly in four quadrants, almost independent of the laser intensity. Two reasons are responsible for this phenomenon. One is that the second electron is emitted randomly along the laser polarization, and the other is that the two electrons cannot be distinguished. Such a feature agrees well with the theoretical prediction by Feuerstein *et al.* [21]. However, the longitudinal momentum distributions of the RII electrons, as shown in Figs. 2(d)–2(f), exhibit notable dependence on the laser intensity. At lower laser intensities, as shown in Fig. 2(d) for 7.5×10^{13} W/cm^2, the electrons occupy almost equally in four quadrants. Because the number of RII electrons at low laser intensities is small, the distribution trend is not clear. Only by the statistical data we find that more electrons distribute in the second and the fourth quadrants. When the laser intensity increases, the emission propensity becomes clear. As shown in Fig. 2(f), four highlighted dots appear in the first and the third quadrants, which forms the finger-like structure in the momentum diagram. More than 60 percents of the RII electrons distribute in the first and the third quadrants. Hence a trend is explicit: The ratio of RII electrons in the first and the third quadrants to that in the second and the fourth quadrants increases with the laser intensity. Correspondingly, the emission of RII electrons transits from anticorrelation to correlation, which results in the above

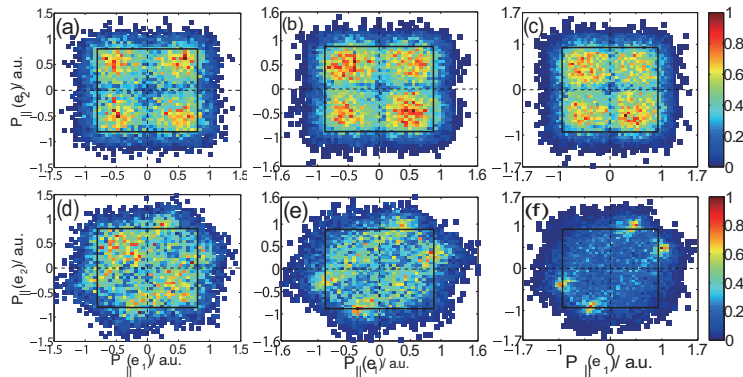transition in the momentum distributions of all NSDI electrons.

Fig. 2. The longitudinal momentum distributions of the RESI electrons (upper row) and the RII electrons (bottom row). Laser intensities are 0.75 (a, d), 0.9 (b, e), and 1.0 (c, f) $\times 10^{14}$ W/cm^2, respectively.

The momentum distribution of Ar^{2+} ions provides a cross evidence to the motion of electrons. We calculate the momentum spectra of Ar^{2+} ions in RII to support the above statement, and some results are shown in Fig. 3. The momentum spectrum for 7.5×10^{13} W/cm^2 displays a single peak at zero, indicating most ions in static state after double ionization. This implies that the two electrons are ejected back-to-back so that the momentum transfer to their parent ion is small. As the laser intensity increases, two flanks around the central peak raise and exceed the peak gradually, so that the momentum distribution of Ar^{2+} ions becomes broad and flat. Finally, two peaks located at the two poles dominate the whole momentum spectrum, as shown for 2.0×10^{14} W/cm^2. This means that almost half of ions move in one direction and the other half of ions move in the opposite direction. This further indicates that the two electrons eject side-by-side so that the recoil momentum of ion is large. The change of the Ar^{2+} ions' recoil momentum distribution provides a substantial support to our judgement that the RII electrons change their emission propensity as the laser intensity increases.
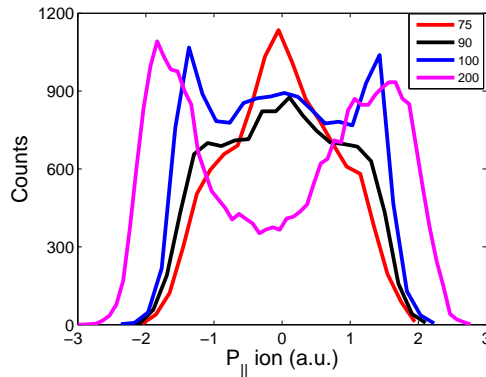

Fig. 3. The momentum distributions of Ar^{2+} ions for the RII process at different laser intensities. The laser intensity marked in the figure is in the unit of 10^{12} W/cm^2.

Why do the RII electrons change their propensity of ejection as the laser intensity increases?

To answer this question, we study the momentum change of RII electrons in the laser pulse. When an electron is released into a laser field, it is accelerated by the electric field and finally gets a drift momentum $\mathbf{P}_{drift}$ as

$$\mathbf{P}_{drift} = \int_{t_i} E(t)dt = -\frac{E_0}{\omega}\sin(\omega t_i), \qquad (4)$$

where t_i denotes the time of ionization. The drift momenta can be regarded as the same for the two RII electrons, because it varies with the time of ionization while the latter differs less in RII. The final momentum of the electron is the sum of the momentum just after the recollision, the drift momentum, and the impulse of the Coulomb force by the core and the other electron. The Coulomb repulsion between electrons prompts the two RII electrons to move back-to-back, while the laser pulse pulls the two electrons to move side-by-side. Shortly after the recollision, the two electrons are still close to each other so that the Coulomb repulsion overcomes the electric force; hence the two RII electrons accelerate in opposite directions for a while. At lower laser intensities, the drift momentum is small, and thus the motion of the electrons is less changed by the laser field. Therefore the two RII electrons eject outside the laser pulse back-to-back with large probability. At higher laser intensities, the drift momentum is large, and thus the motion of the electrons is greatly changed by the laser field, hence more electrons eject out the laser pulses side-by-side. Here the Coulomb attraction of the parent core is out of consideration due to the long distance to the emitted electrons during the recollision process.
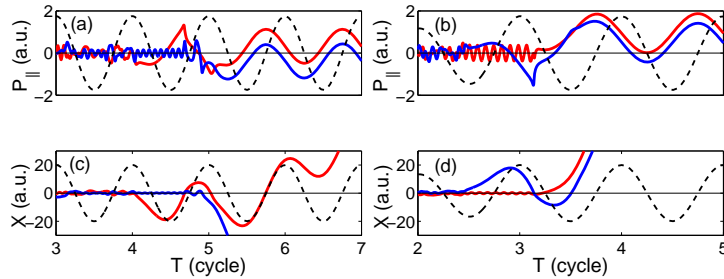

Fig. 4. The longitudinal momenta and trajectories of the two electrons in the laser pulses of intensities 7.5×10^{13} W/cm^2 (left column) and 1.0×10^{13} W/cm^2 (right column). The dot lines indicate the electric field of the laser pulses.

The above statements are illustrated in Fig. 4, which depicts the evolution of the trajectory and the momentum of electrons for two laser intensities. For a lower laser intensitys shown in the left column, recollision occurs at about $4.7T$. The two electrons separate promptly after recollision, due to the Coulomb repulsive force, and leave outside the laser pulse in opposite directions. For higher laser intensities, the drift momentum becomes large. As shown in the right column for 1.0×10^{14} W/cm^2, the two electrons moves into opposite directions shortly after recollision. However, the laser pulse changes the motion of the second electron and finally drives the two electrons moving outside in the same direction. It should be mentioned that not all electrons change their motion as the above manner, because their motion also depends on the initial states of the electrons.

In order to identify the influence of the Coulomb force between the two RII electrons, in Fig. 5 we illustrate the longitudinal momentum distributions at different moments. Statistical data show that most RII electrons collide at about $5.0T$ for 7.5×10^{13} W/cm^2, and collide at about $3.0T$ for 2.0×10^{14} W/cm^2. We then depict the longitudinal momentum distributions
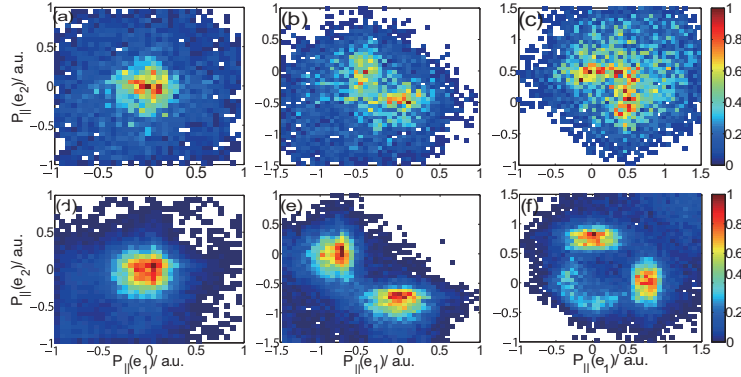
Fig. 5. The longitudinal momentum distributions calculated at 7.5×10^{13} W/cm^2 (a-c) and 2.0×10^{14} W/cm^2 (d-f) at different moments: (a) $5.0T$, (b) $5.1T$, (c) $5.6T$, (d) $3.0T$, (e) $3.1T$, and (f) $3.6T$, respectively.

at these two intensities at $5.0T$ and $3.0T$ in Figs. 5(a) and 5(d), respectively. Each panel exhibits a highlighted area located at the center of the blue background. This indicates that, just after recollision, most electrons have small momenta and hence the momentum distributions are similar for different laser intensities. Shortly after the recollision, both the momentum distributions, shown in Figs. 5(b) and 5(e), exhibit two well separated bright areas. This indicates that the momentum changes distinctively during a short time after recollision. Although the two electrons are still close to each other so that the Coulomb repulsion is strong, the effect of Coulomb repulsion can not be identified evidently, because the electric fields approach their peak values. However, when the electric field inverses after a half optical period, the momentum distributions exhibit some new features, from which the effect of the Coulomb repulsion can be identified. The momentum distribution, as shown in Fig. 5(f) for 2.0×10^{14} W/cm^2 calculated at $3.6T$, is quite similar to but is antiphase with its counterpart at $3.1T$. This indicates the laser field steering the motion of the two RII electrons, because the momentum distribution varies as the electric field does. However, the bright area in the momentum distribution for a lower laser intensity, shown in Fig. 5(c) calculated at $5.6T$, is antiphase with but is narrower and brighter than the highlighted area in $5.1T$. Besides this area, broad light-green areas are notable. This area locates around the highlighted region and takes over a large proportion of the diagram. This indicates that more electrons move deviating from the laser polarization so that the momentum diagram becomes more uniformly distributed. This difference reveals the effect of Coulomb repulsion between the two RII electrons.

4. Conclusions

We study NSDI of Ar atoms by a classical ensemble method. The RESI electrons and the RII electrons are studied separately. When the laser intensity increases, the RESI electrons always distribute uniformly in four quadrants of the momentum diagram, while the RII electrons change their emission priority from anticorrelation to correlation. The Coulomb repulsion between the two RII electrons is responsible for this change. At lower laser intensities, the Coulomb repulsion dominates the motion of electrons and pushes them leaving the laser field back-to-back. At higher laser intensities, the effect of the Coulomb repulsion is suppressed and the drift momentum obtained from the laser field dominates the motion of electrons. The drift momentum drives them leaving the laser field side-by-side. The transition in the electron emission reveals a strong electron-electron correlation in intense laser pulses.

Acknowledgments